

See discussions, stats, and author profiles for this publication at: <https://www.researchgate.net/publication/41560898>

Homodimerization of the p51 Subunit of HIV-1 Reverse Transcriptase

ARTICLE *in* BIOCHEMISTRY · FEBRUARY 2010

Impact Factor: 3.02 · DOI: 10.1021/bi902116z · Source: PubMed

CITATIONS

9

READS

21

5 AUTHORS, INCLUDING:



Xunhai Zheng

National Institute of Environmental Health S...

22 PUBLICATIONS 91 CITATIONS

[SEE PROFILE](#)



Geoffrey Andrew Mueller

National Institute of Environmental Health S...

75 PUBLICATIONS 1,924 CITATIONS

[SEE PROFILE](#)

Homodimerization of the p51 Subunit of HIV-1 Reverse Transcriptase[†]

Xunhai Zheng, Geoffrey A. Mueller, Matthew J. Cuneo, Eugene F. DeRose, and Robert E. London*

Laboratory of Structural Biology, MR-01, National Institute of Environmental Health Sciences, National Institutes of Health,
Research Triangle Park, North Carolina 27709

Received December 10, 2009; Revised Manuscript Received February 24, 2010

ABSTRACT: The dimerization of HIV reverse transcriptase (RT), required to obtain the active form of the enzyme, is influenced by mutations, non-nucleoside reverse transcriptase inhibitors (NNRTIs), nucleotide substrates, Mg ions, temperature, and specifically designed dimerization inhibitors. In this study, we have utilized nuclear magnetic resonance (NMR) spectroscopy of the [*methyl*-¹³C]methionine-labeled enzyme and small-angle X-ray scattering (SAXS) to investigate how several of these factors influence the dimerization behavior of the p51 subunit. The ¹H-¹³C HSQC spectrum of p51 obtained at micromolar concentrations indicates that a significant fraction of the p51 adopts a “p66-like” conformation. SAXS data obtained for p51 samples were used to determine the fractions of monomer and dimer in the sample and to evaluate the conformation of the fingers/thumb subdomain. All of the p51 monomer observed was found to adopt the compact, “p51C” conformation observed for the p51 subunit in the RT heterodimer. The NMR and SAXS data indicate that the p51 homodimer adopts a structure that is similar to the p66/p51 heterodimer, with one p51C subunit and a second p51 subunit in an extended, “p51E” conformation that resembles the p66 subunit of the heterodimer. The fractional dimer concentration and the fingers/thumb orientation are found to depend strongly on the experimental conditions and exhibit a qualitative dependence on nevirapine and ionic strength (KCl) that is similar to the behavior reported for the heterodimer and the p66 homodimer. The L289K mutation interferes with p51 homodimer formation as it does with formation of the heterodimer, despite its location far from the dimer interface. This effect is readily interpreted in terms of a conformational selection model, in which p51_{L289K} has a much greater preference for the compact, p51C conformation. A reduced level of dimer formation then results from the reduced ratio of the p51E_{L289K} to p51C_{L289K} monomers.

HIV-1 reverse transcriptase (RT)¹ has emerged as a central target for drug intervention in the treatment of AIDS (1, 2). It plays a pivotal role in HIV replication by converting single-stranded genomic RNA into double-stranded proviral DNA. The enzyme is composed of two subunits, p66 and p51, with the polymerase and RNase H active sites located in the p66 subunit. The p51 subunit is identical in sequence to p66 but lacks the C-terminal RNase H domain and adopts a very different conformation in the heterodimer. Studies utilizing an RT mutation that interferes with dimerization support the sequential processing of an initially formed p66 homodimer, followed by proteolytic processing to yield the mature, p66/p51 heterodimer (3). The dimerization of HIV reverse transcriptase has been of interest

since it can be significantly influenced by non-nucleoside RT inhibitors (NNRTI) and is therefore presumably related to their mechanism of action (4–6). Because drug-resistant strains of RT continue to evolve, the development of dimerization inhibitors has been an active area of research (7–14).

The dimerization of HIV reverse transcriptase is influenced by mutations (15–25), nucleotide substrates (26), temperature, magnesium, and other solution conditions (8, 26–29). For residues located at or near the dimer interface, the effect of the mutation on dimer stability is readily interpreted, while for other mutations, the effect appears to be more indirect. Among the dimerization-interfering mutations, L289K is one of the most counterintuitive (15). The L289₅₁ residue in RT is positioned at the dimer interface and makes multiple hydrophobic contacts with residues on the p66 subunit, while the L289₆₆ residue is a surface-exposed residue located at the tip of the thumb subdomain, far from the interface. Unexpectedly, the L289K₆₆ mutation strongly interferes with dimerization, while the L289K₅₁ mutation is benign (15). If the structure of the RT heterodimer is used as a model for the p51 homodimer, neither of the L289 residues is positioned near the dimer interface. In addition to the surprising effects of the L289K mutation on dimerization behavior, results for the p51 homodimer dissociation constant (5, 27) and for the effects of the NNRTI nevirapine on dimer formation (4, 30, 31) have been inconsistent. The p51 homodimer has been reported to exhibit approximately half the activity and processivity of the RT heterodimer (32); however, it is well-known that the

[†]This research was supported by the Intramural Research Program of the National Institute of Environmental Health Sciences (NIEHS). E.F.D.’s contribution was funded in whole with Federal funds from NIEHS, under Delivery Order HHSN273200700046U to SRA International, Inc. This research was supported by Research Project Z01-ES050147 (R.E.L.) in the Intramural Research Program of the National Institutes of Health.

*To whom correspondence should be addressed: NIEHS, 111 T. W. Alexander Dr., P.O. Box 12233, Research Triangle Park, NC 27709. Telephone: (919) 541-4879. Fax: (919) 541-5707. E-mail: london@niehs.nih.gov.

¹Abbreviations: RT, reverse transcriptase; IPTG, isopropyl thio-D-galactoside; HSQC, heteronuclear single-quantum coherence; DSS, 2,2-dimethylsilapentane-5-sulfonic acid; NNRTI, non-nucleoside RT inhibitors; NMR, nuclear magnetic resonance; SAXS, small-angle X-ray scattering.

primer/template substrate used for activity measurements significantly promotes dimerization (8, 26, 29, 33), and p51 activity shows a particular sensitivity to the nature of the substrate used.

In this study, we have utilized biophysical techniques that directly probe the solution behavior of p51. We have extended our use of [$\text{methyl-}^{13}\text{C}$]methionine labeling to understand conformational aspects of the dimerization process for the p51 subunit. The dependence of the methionine methyl resonances on subunit conformation provides a useful basis for characterizing the conformational heterogeneity of the p51 homodimer. Application of the SAXS technique to the characterization of the p51 solutions has been found to be particularly valuable, both for quantifying the monomer:dimer ratio and for evaluating the open versus closed conformational preferences of the fingers/thumb subdomains. Previous evaluations of this ratio required considerably more involved and invasive procedures, such as spin labeling of the protein (34). On the basis of these studies, we have also developed a conformational selection model that provides a more physically intuitive basis for understanding how some mutations and NNRTIs can influence the dimerization process. This approach allows analysis of effects that arise not from a direct perturbation of the dimer interface but rather from a change in the conformational preferences of the p51 monomer.

MATERIALS AND METHODS

Materials. Oligonucleotides used as PCR primers for site-directed mutagenesis were purchased from Integrated DNA Technologies. Unlabeled amino acids, Q-Sepharose FF, and the ssDNA cellulose matrix were purchased from Sigma-Aldrich. [$\epsilon\text{-}^{13}\text{C}$]Methionine was obtained from Cambridge Isotope Laboratories. Isopropyl thio- β -galactoside (IPTG) was from Invitrogen. The HiLoad 26/60 Superdex 200 column was from Amersham Pharmacia Biotech AB.

Plasmids pET21a (+) p66 and pET30a (+) p51 were a gift from the laboratory of S. Wilson (National Institute of Environmental Health Sciences). The p51 construct terminates at W426. Mutagenesis studies were conducted by using the QuickChange XL site-directed mutagenesis kit (Stratagene). The desired mutated gene sequences were confirmed by DNA sequence analysis. The two expression plasmids were transformed into *Escherichia coli* BL21(DE3) codon plus RIPL, and protein expression was induced for 4 h at 37 °C by addition of 0.5 mM IPTG into the culture, when the OD₆₀₀ value reached 0.8–1. The mutants constructed for these studies included M16L, M230L, M230L/M357L, C280S, and L289K.

Sample Preparation. For the purpose of NMR studies, each mutant of p51 was expressed at 37 °C using enriched medium (PAG) (35) containing 17 unlabeled amino acids (no C, Y, and M), with [$\epsilon\text{-}^{13}\text{C}$]methionine, which is expected to repress the endogenous synthesis of methionine by the bacteria (36). The purification of the samples was identical to that previously described (37, 38). Briefly, no affinity tags were used so three columns were used for purification: cation exchange followed by an ssDNA cellulose column and finally size-exclusion chromatography.

The final samples were exchanged into NMR buffer [10 mM Tris-HCl- d_{11} (pD 7.6), 200 mM KCl, 1.5 mM sodium azide, 4 mM MgCl₂, and 100 μM 2,2-dimethylsilapentane-5-sulfonic acid (DSS) as an internal chemical shift standard, in D₂O] using a PD-10 desalting column (Pharmacia) and further concentrated to approximately 50 μM. The concentration of each sample was

determined by UV absorbance. The use of at least 200 mM KCl was determined to be important for the long-term stability of the samples required for the NMR investigations. Use of lower salt concentrations resulted in gradual precipitation of the protein.

NMR Spectroscopy. All NMR experiments were performed at 25 °C using a Varian UNITY INOVA 500 MHz NMR spectrometer, equipped with a 5 mm Varian (500 MHz) ¹H{¹³C,¹⁵N} triple-resonance cryogenically cooled probe, with actively shielded z-gradients. We used the Varian gChsqc experiment included in Biopack with the phase-cycling option. The acquisition parameters for all experiments were as follows: 64 transients, 64 ms acquisition, 1 s relaxation delay with 1024 points, and sweep width of 14 ppm. In the indirect dimension, 128 points were acquired with a sweep width of 11 ppm, and the ¹³C offset was set to 17 ppm. All NMR data were processed using NMRPipe (39) and analyzed with NMRviewJ (40).

Size-Exclusion FPLC Analysis. SEC-FPLC was performed at room temperature on an Akta FPLC system using a SuperdexTM 200 10/300 GL column (Amersham Bioscience). Protein samples (100 μL) were loaded and eluted with running buffer [50 mM Tris-HCl and 200 mM NaCl (pH 8.0)] at a flow rate of 0.75 mL/min. Data are presented for the following samples: 43 μM p51, 43 μM p51 in the presence of nevirapine, 80 μM p51_{L289K}, 50 μM p51_{L289K} with nevirapine, and 15 μM RT, used as a control. The elution profiles were recorded at 280 nm after the column had been pre-equilibrated with running buffer.

SAXS Data and Analysis. SAXS spectra were recorded at National Synchrotron Light Source beamlines X21 and X9 (Brookhaven National Laboratory, Upton, NY). The wavelengths of the beams were 1.24 and 0.855 Å, respectively. For the SAXS analysis, protein was dialyzed into 50 mM Tris-HCl (pH 8.0) and 200 mM KCl with either no magnesium or 4 mM MgCl₂, as indicated. The recorded intensity of each sample was circularly averaged and scaled to produce a relative scattering intensity, $I(\mathbf{q})$, where the momentum transfer vector $\mathbf{q} = 4\pi \sin\theta/\lambda$, after subtraction of buffer scattering contributions. SAXS data were collected at protein concentrations of 1–6 mg/mL. Background subtraction, averaging, and scaling were conducted with Primus (41).

CRYSTOL was used to compare the SAXS-based intensity data with theoretical intensity data derived from the atomic structures obtained from X-ray crystallographic studies (42). Additionally, the scattering data were analyzed according to the method of Svergun and co-workers, using OLIGOMER to compute the fraction of structures present with known scattering (41). This procedure assumes that the macromolecule(s) present in the cell can adopt a limited number of predetermined structures or conformations and seeks to optimize the fit of the experimental scattering curve by varying the fractional contributions of the scattering curves calculated for each component structure. The success of this approach is dependent on how well the assumed conformational ensemble covers the set of conformations present in solution. Three models were considered for isolated p51, as shown in Figure 1. In the first model, p51 adopts a compact globular conformation identical to its conformation, p51C, in the RT heterodimer (Figure 1a). The isolated p51 subunit was also allowed to adopt two alternate, extended conformations similar to those observed for the first 426 residues of the p66 subunit in the heterodimer, here termed p51E_{open} and p51E_{closed}. For the first model, the fingers and thumb were positioned in an open conformation, as observed in RT–NNRTI complexes such as

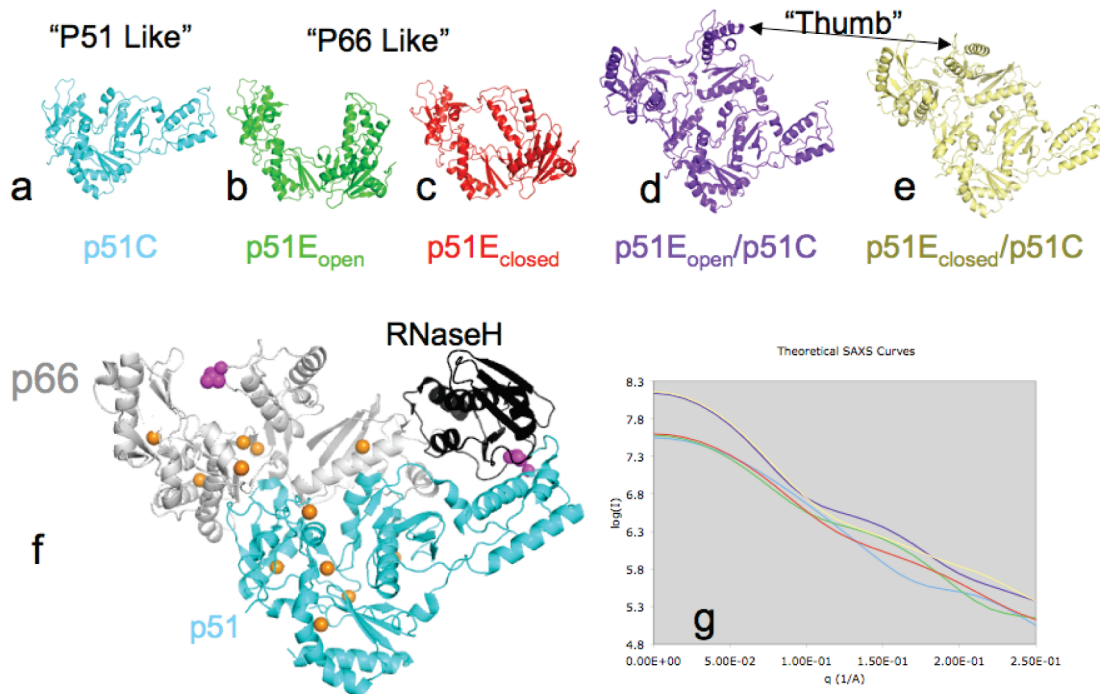


FIGURE 1: Structures of RT and predicted SAXS parameters. The structures in panels a–e were used to predict the SAX scattering profiles in panel g. The color coding of the SAXS curves in panel g is identical to the coloring of the structures in panels a–e. A detailed discussion of the component structures is contained in the text. Panel f shows PDB entry 3DLK with p51 colored cyan and p66 colored white except for the RNase H domain which is colored black. Orange spheres indicate the positions of the methyl group of the methionine residues. The side chain of L289 is shown with magenta spheres.

Protein Data Bank (PDB) entry 2VG5 (43) (Figure 1b), while in the second model, the thumb and fingers were positioned in a closed conformation, as observed in PDB entry 3DLK (44) (Figure 1c). Two structures for the p51 homodimer were also included in the structural ensemble. The p51 homodimer was modeled by truncating the p66 subunit at residue 426 and allowing the fingers/thumb conformation to be either open, p51E_{open}/p51C (Figure 1d), or closed, p51E_{closed}/p51C (Figure 1e). All structures lack the RNase H domain of the p66/p51 RT heterodimer (Figure 1f). The theoretically predicted SAXS curves are shown in Figure 1g. The intensity and inflection of these contributions differ sufficiently to support the feasibility of a conformational deconvolution of the SAXS data. The lines are color-coded with respect to the structures shown in Figure 1a–e.

The following main assumptions were made in the analysis given above. (1) The actual structural ensemble present in solution can be described as a mixture of these five component structures only. (2) We neglect any dynamic aspects of these structures. (3) The p51E and p51E/p51C dimer structures can be modeled by dropping the RNase H domain from the corresponding p66/p51 heterodimer structures. Removal of the RNase H domain to create the p51E/p51C homodimer structure eliminates the RNase H interfaces with the connection domain in p51E, and with the thumb domain of p51C. The loss of these interactions might lead to some additional destabilization and conformational heterogeneity. The experimental support for this approach is based on (1) the low χ^2 values obtained for the analyses over a broad range of experimental conditions and (2) the qualitative consistency of the results with the effects of concentration, nevirapine, acetonitrile, and Mg predicted from the literature describing the behavior of p51, p66, and the p66/p51 heterodimer.

Equilibrium Modeling. Numerical evaluation of the sets of equilibrium equations presented in this study was performed using Mathematica (Wolfram Research, Champaign, IL), and following an approach similar to that described by Venezia et al. (5). Briefly, solutions of the simultaneous algebraic equations describing the equilibria were obtained using the Solve and Evaluate commands.

Nomenclature. Subscripts have been used to denote the subunit involved when there is any possibility of ambiguity; e.g., M184₆₆ refers to residue M184 in the p66 subunit. We have also introduced the nomenclature p51C, to describe the p51 monomer in that compact, globular conformation that it adopts in heterodimeric RT, and p51E, to describe the extended, p66-like conformation that it can adopt when it forms a p51 homodimer. We thus refer to the p51 homodimer structure as p51E/p51C, analogous to the p66/p51 nomenclature used for the heterodimer. When a specific conformation of the fingers/thumb subdomain is also indicated, the structure is further identified as p51E_{open}, p51E_{closed}, p51E_{open}/P51C, etc.

RESULTS

NMR Characterization of RT and p51 in Solution. Figure 2 compares the ^1H - ^{13}C HSQC spectra of HIV-1 RT containing [$\text{methyl-}^{13}\text{C}$]methionine in either the p66 or p51 subunit, with the spectra obtained for p51 alone. The resonances for four of the six methionine methyl groups have been assigned previously (38), while the resonances for two residues with a very low degree of solvent exposure, M41 and M164, are not readily observed as a result of greater dipolar broadening. The enzyme contains two active site methionine residues, M184, a component of the active site YMDD motif, and M230, located on the primer grip and positioned to make direct contact with the primer terminus of the DNA substrate. On the basis of crystal structures

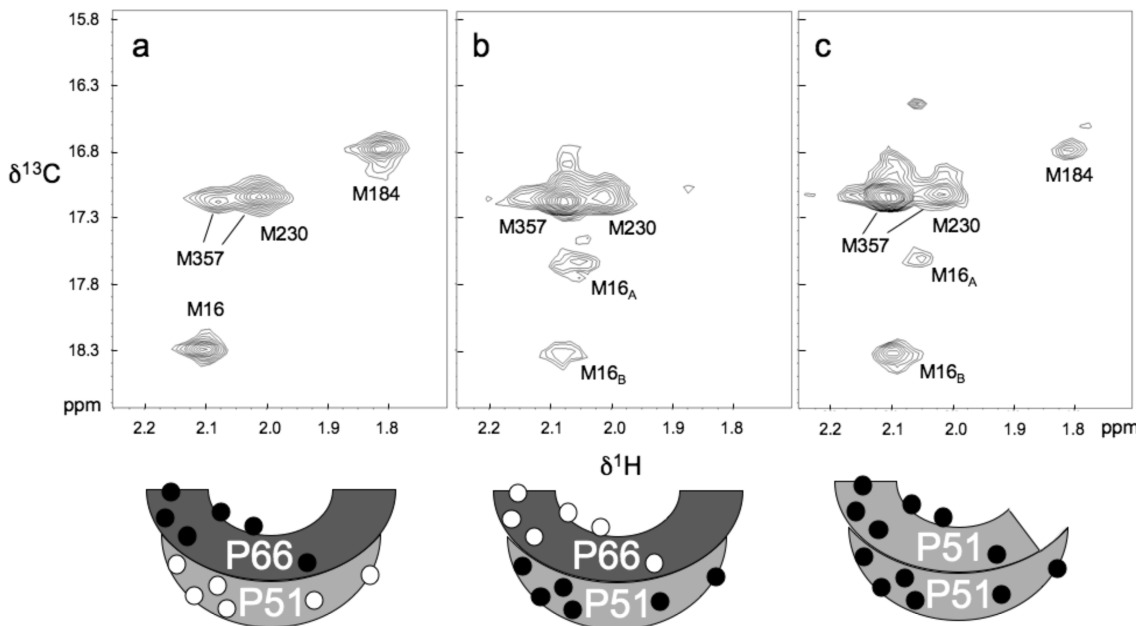


FIGURE 2: ^1H - ^{13}C HSQC spectra of (a) $57 \mu\text{M}$ [$\text{methyl-}^{13}\text{C}$]methionine₆₆ RT, (b) $50 \mu\text{M}$ [$\text{methyl-}^{13}\text{C}$]methionine₅₁ RT, and (c) $30 \mu\text{M}$ [$\text{methyl-}^{13}\text{C}$]p51 subunit. All samples were dissolved in NMR buffer [10 mM Tris-HCl- d_{11} (pD 7.6), 200 mM KCl, 1.5 mM sodium azide, 4 mM MgCl₂, and 100 μM DSS as an internal chemical shift standard, in D₂O]. Spectra were recorded at 25 °C. Schematic figures at the bottom indicate the subunit labeling pattern, with filled circles indicating [$\text{methyl-}^{13}\text{C}$]methionine labeling. The spectra of the p66/p51 heterodimer preparations shown in panels a and b are reproduced from panels a and b of Figure 2 of ref 38. Preparation of the selectively labeled RT heterodimer is described in that reference.

of RT, the environment of these two residues is expected to be very different in the two subunits, so that the NMR parameters are expected to show a corresponding subunit dependence. The M184 resonances show the expected dependence (Figure 2a,b), with M184₅₁ not readily visible as a result of the shorter T_2 value characterizing the buried residue, while the M230 resonances appeared to be similar in both subunits. We note that segments of the protein containing M230 were disordered in three of four p51 subunits and one p66 subunit in crystal structures of the apoenzyme, so that the observation may be biased toward the observation of the disordered species (38).

The other assigned methionine resonances, corresponding to residues M16 and M357, exhibit two resonances each, with characteristics that are also subunit-dependent. Confirmation of the M16 assignments is provided by spectra of the p51_{M16} mutant shown in Figure 3a, in which both M16 resonances have been eliminated. In the p66 subunit, the intensity of M16_A is much greater than that of M16_B, while in p51, the intensities of the two component resonances are more similar (Figure 2). Finally, M357 also was found to produce two resonances, with M357_A much more intense in the p51 subunit than in p66 (38). This difference, as well as the two observed component resonances, appears to be related to the proximity of M357₆₆ to the subunit interface. The segment containing M357₅₁ is disordered in two of the reported crystal structures of the apoenzyme, and the segment containing this residue is probably highly mobile in the p51 subunit, explaining its high intensity.

The assignments described above provide a basis for interpretation of the spectrum obtained for the isolated [$\text{methyl-}^{13}\text{C}$]methionine p51 subunit, which can exist in solution as either a monomer or a dimer. On the basis of a recently determined p51 homodimer dissociation constant of $230 \mu\text{M}$ measured at 5 °C, we initially estimated that at $30 \mu\text{M}$ p51 this sample should be ~90% monomer and 10% dimer (5). The most striking feature of the HSQC spectrum obtained for the [$\text{methyl-}^{13}\text{C}$]methionine p51

sample is the appearance of a reasonably intense resonance with ^1H and ^{13}C resonance shifts identical to those observed for M184₆₆ in the heterodimer (cf. Figure 2a,c). In combination with the homodimer dissociation constant given above, this observation supports the conclusion that a substantial fraction of the p51 monomer adopts an extended, p66-like conformation, rather than the compact globular structure observed for p51 in the RT heterodimer. In contrast, the strong intensity of the M357 resonance is more similar to that observed for the p51 subunit of RT, supporting the opposite conclusion. However, a quantitative examination of the relative resonance intensities of the p51 sample, normalized using the total M16 resonance intensity, indicates that they approximate an average of the intensities observed for equal concentrations of the p66 and p51 subunits (Table 1). Thus, the evidence of the HSQC spectrum supports the conclusion that even at a concentration of $30 \mu\text{M}$, most of the sample exists as a p51 homodimer that is a conformational heterodimer. In particular, the intensities of the M184 and M16 resonances closely approximate the average values expected if the p51 subunit adopts the two different tertiary structures with equal probability.

As a related technical point, we wish to address the potential spectral consequences of contaminant unfolded or partially unfolded protein. One limitation on the use of [$\text{methyl-}^{13}\text{C}$]methionine as an NMR probe is the frequent appearance of a significant resonance or group of resonances with shift values near $\delta^1\text{H} = 2.05 \text{ ppm}$ and $\delta^{13}\text{C} = 17.0 \text{ ppm}$ that result from the presence of some soluble denatured protein. Such resonances can be observed in many of the reported spectra of methionine-labeled enzymes. As a result of the high internal mobility of the methionine residues and the tendency of all of the methionine residues of the denatured protein to resonate at similar shifts, the corresponding resonance intensity of a relatively small fraction of denatured protein can be significant. Since the M357 resonance, which has a high degree of solvent exposure, is near this position,

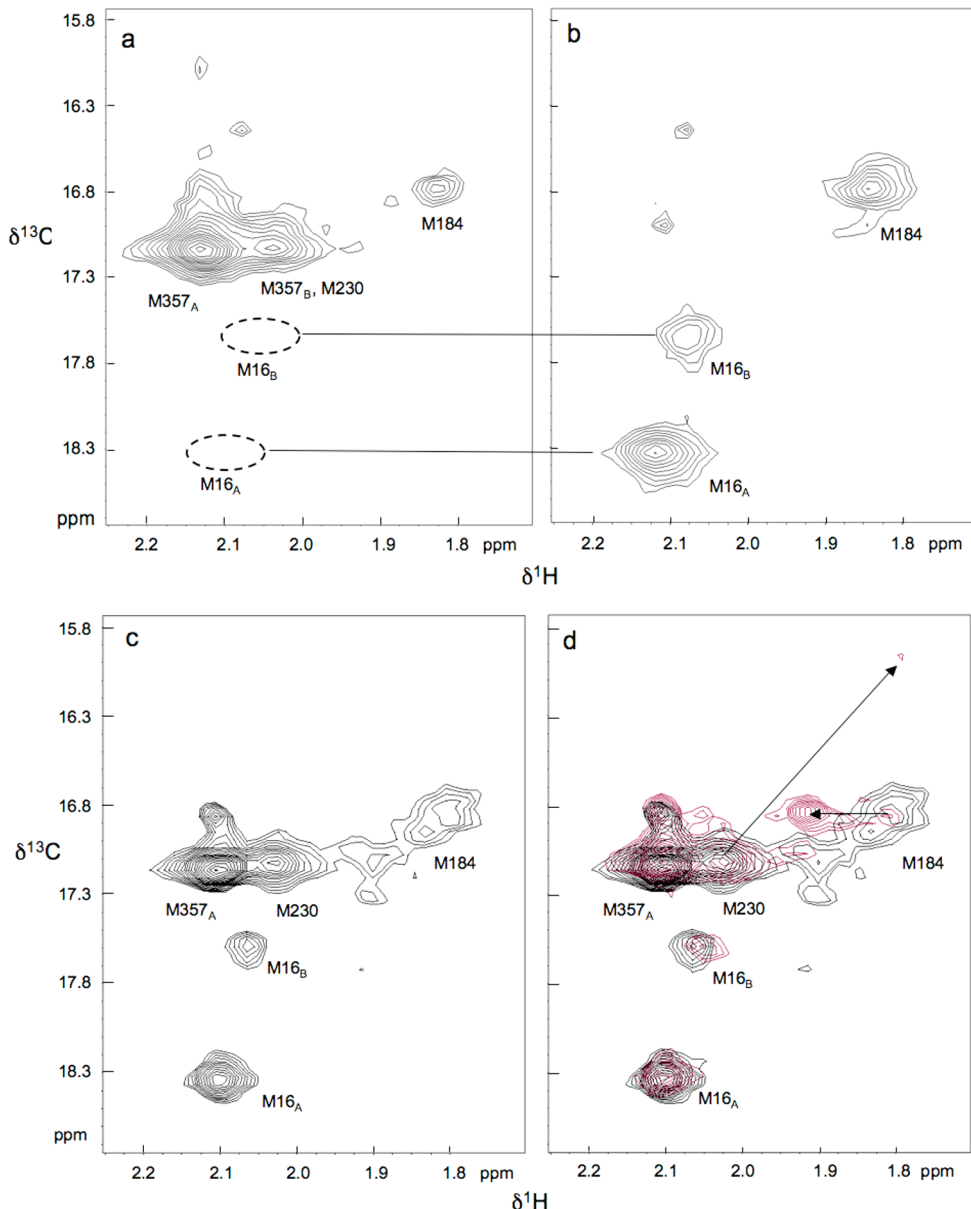


FIGURE 3: ^1H - ^{13}C HSQC spectra of [$\text{methyl-}^{13}\text{C}$]methionine p51 mutants: (a) M16L, b) M230L/M357L, (c) L289K, and (d) L289K (black) and L289K with nevirapine (red). The arrows in panel d indicate nevirapine-induced shifts. Residue M16 produces two resonances, labeled M16_A and M16_B , with the $\text{M16}_A:\text{M16}_B$ ratio considerably higher in p66 and p51E subunits than in the p51C subunit. The M357 residue in the p51C subunit also produces two resonances, one of which, M357_B , overlaps with M230. The intensity of the M357_B resonance appears to be related to the proximity of M357 to the dimer interface. Temperature and buffer conditions were as described in the legend of Figure 2.

Table 1: Normalized Intensities of p51 Resonances

	p66/p51 ^a	p51	L289K p51	L289K p51 with NVP
M16	1.0	1.0	1.0	1.0
M41	—	—	—	—
M164	—	—	—	—
M184	0	0.45	0.21	0.50
M230	1.4	0.89	0.69	0.52
M357	4.1	3.24	2.8	3.0

^aResonance intensities for [$\text{methyl-}^{13}\text{C}$]methionine₅₁ RT are normalized relative to the total intensity of both M16 resonances.

we also obtained a spectrum of the doubly mutated [$\text{methyl-}^{13}\text{C}$]methionine p51_{M230L/M357L} (Figure 3b). As one can plainly see in Figure 3, the only significant resonances that remain correspond to M184 in a p66-like environment, and to M16, presumably

arising from the p51 subunits in both the p66-like and p51-like conformations. Hence, this observation supports the conclusion that the M357 resonance contains at most a very small contribution from the unfolded protein.

SAXS Analysis of p51. SAXS data were obtained on p51 solutions under various conditions, as described in Materials and Methods. Our analysis assumes that in all cases the sample contained an undetermined mixture of five structures, three monomers and two dimers as described in Materials and Methods and illustrated in Figure 1. Figure 4 shows two examples of the fit of the linear combinations of the predicted scattering profiles with the experimental data using OLIGOMER (41). In both cases shown here, the fit is very good ($\chi^2 = 4.8$ and 3.1) in the range of long vectors and somewhat poorer in the highest-resolution range, which is typical for SAXS fits.

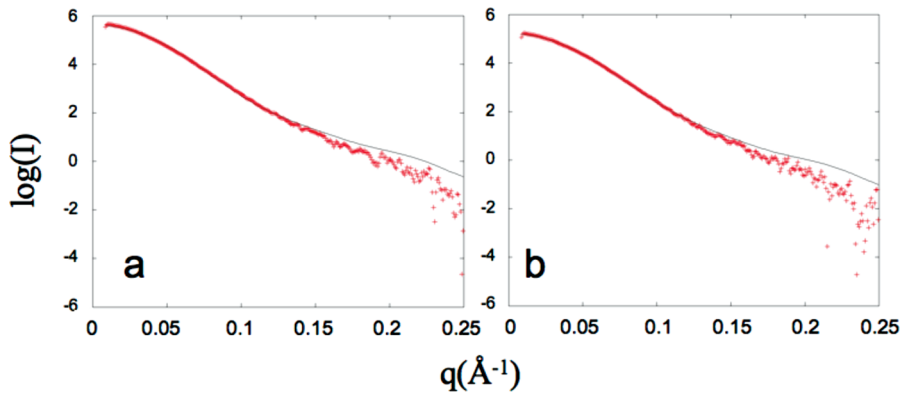


FIGURE 4: SAXS scattering profiles analyzed with OLIGOMER. The experimental SAXS data are indicated with plus signs, and the fit of a linear combination of predicted scattering profiles is drawn with a black line for (a) $60\text{ }\mu\text{M}$ p51 and (b) $40\text{ }\mu\text{M}$ p51. The χ^2 values of the fit are 4.8 and 3.1 for panels a and b, respectively. All other SAXS fits are displayed in the Supporting Information.

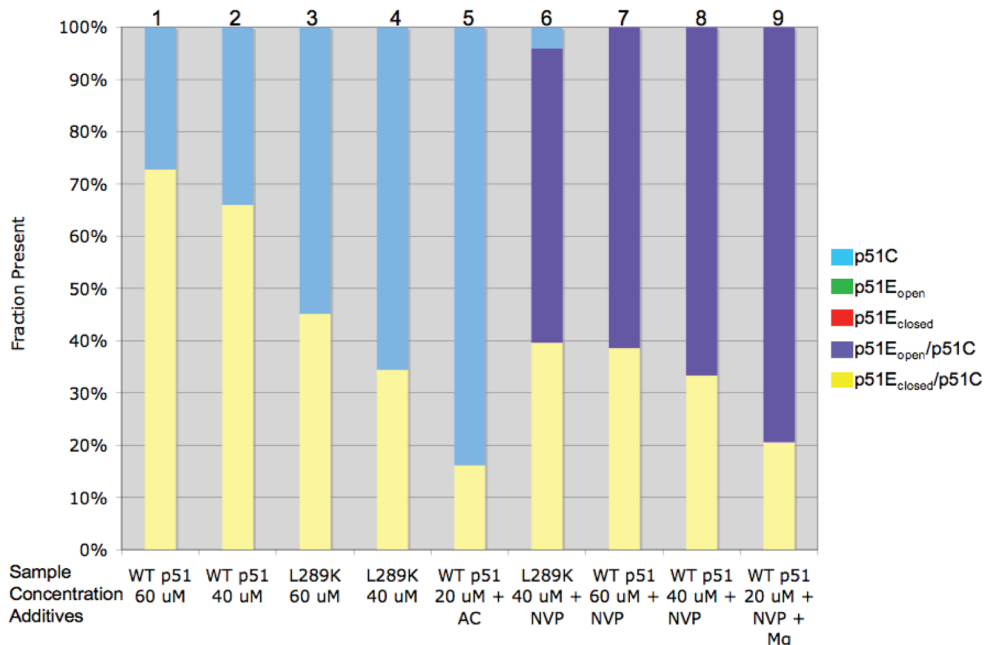
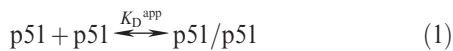


FIGURE 5: Fraction of p51 models present in solution. On the basis of OLIGOMER analysis of SAXS data, the fraction of each p51 model present is shown in a bar graph, with the total set to 100%. Results of the analysis for each sample are summarized in a table included as Supporting Information. Each column is a different sample indicated at the bottom of the figure. The bars are colored to be similar to the structures shown in Figure 1. No p51E monomer, either open (green) or closed (red), was found in the analysis. The additives indicated at the bottom of the columns are 4 mM MgCl_2 (Mg), 0.5 mM nevirapine (NVP), and 10% acetonitrile (AC). All samples were dissolved in 50 mM Tris-HCl and 200 mM KCl (pH 8.0).

Figure 5 summarizes the fractional percent of each component structure present in solution under the conditions indicated on the basis of the analysis of the SAXS data. For the sake of clarity, the color coding of the structures in Figure 1 is the same as the bars in Figure 5. The fits indicate that a sample containing $60\text{ }\mu\text{M}$ p51 has a monomer:dimer ratio of $\sim 1:3$ and that all of the dimer present adopts a closed fingers/thumb subdomain orientation. No significant contributions were observed for each of the three other structures allowed by the modeling. At a slightly lower concentration ($40\text{ }\mu\text{M}$ p51), the monomer:dimer ratio increases to $\sim 1:2$ and the fingers/thumb orientation remains closed. Using a simple monomer–dimer equilibrium analysis described by the relation



the data in columns 1 and 2 of Figure 5 correspond to a K_D^{app} value of $\sim 4\text{ }\mu\text{M}$, while the data in columns 3 and 4 for p51_{L289K}

correspond to a K_D^{app} of $\sim 36\text{ }\mu\text{M}$, a 9-fold increase. The qualitative effects of concentration, nevirapine, and the L289K mutation on conformation and on the monomer:dimer ratio, discussed in greater detail below, are all consistent with expectations based on the related dimerization literature. These results confirm the interpretation of the NMR spectra, which imply that a substantial amount of dimer is present. These K_D^{app} values are substantially lower than a recent reported value of $230\text{ }\mu\text{M}$ (5), reflecting the hypersensitivity of the dimerization process on the experimental conditions.

Effect of the L289K Mutation and Acetonitrile on the p51 Monomer–Dimer Equilibrium. Many studies have identified mutations that influence heterodimer stability (15–25). The effects of the L289K mutation were of particular interest, since this mutation is located far from the dimer interface, particularly in the case of the p51 homodimer (Supporting Information). The effects of the L289K mutation on the behavior of p51 were

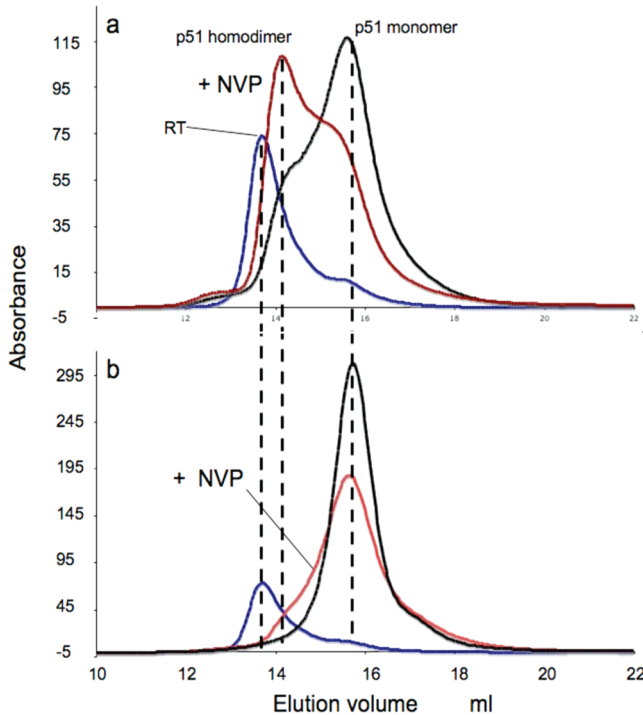


FIGURE 6: Size-exclusion chromatography profiles. (a) p51 in the absence (black) or presence (red) of nevirapine. (b) p51_{L289K} in the absence (black) or presence (red) of nevirapine. For reference, the RT elution profile is indicated with a blue line. Maximum elution positions for the p51 monomer, p51 dimer, and RT heterodimer are indicated by dashed lines.

examined using NMR, SAXS, and size-exclusion chromatography. The HSQC spectrum of [*methyl-¹³C*]methionine p51_{L289K} shows many of the features seen for wild-type (wt) p51; however, the M184 resonance is broader and weaker than that observed for the p51 homodimer (Figures 2c and 3c). In addition, the high intensity of the M357 resonance is more similar to that exhibited by the spectrum of the p51 subunit of the RT heterodimer (38). These results are consistent with a greater fraction of the p51 monomer, as predicted for the dimerization deficient L289K mutant, although we emphasize that in this case, the interpretation of the spectral characteristics is not unique. OLIGOMER analysis of the SAXS data summarized in Figure 5 yields results that are generally consistent with the analysis of the NMR spectra. The fractional percentages and the χ^2 of each fit are given in the Supporting Information. As is apparent from a comparison of columns 1 and 2 with columns 3 and 4 of Figure 5, p51_{L289K} is significantly more monomeric than wt p51 at equivalent concentrations. Again, there are no detectable conformations that resemble a p51E monomer in either the open or closed conformation or p51 dimer with an open thumb conformation. The conclusions derived from size-exclusion chromatographic analysis are generally consistent with the expected results, demonstrating that L289K p51 elutes at the same time as monomeric p51 (Figure 6). Under the conditions of the chromatography study, the addition of nevirapine produced only a small increase in the fraction of p51 homodimer. The chromatographic results generally indicated lower dimer fractions, presumably as a consequence of sample dilution.

It also has been reported that acetonitrile is capable of producing subunit dissociation without producing a significant degree of unfolding (27, 29). We assessed the effect of acetonitrile on p51 structure by both NMR and SAXS. For the NMR studies, the M357_B resonance, which we have previously found to

be sensitive to dimer formation, is unfortunately degenerate with that of M230. For this reason, we used [*methyl-¹³C*]methionine p51_{M230L} to eliminate the overlap and better evaluate its position. A reduction in the intensity of the M357_B resonance was observed, consistent with this type of dissociation (spectra included as Supporting Information). There is also an observed broadening and some loss of intensity of the M184 resonance, which would be consistent with a reduction in the amount of p51E conformation present as either a monomer or dimer. The fact that a significant M184 resonance remains evident even in the presence of 10% acetonitrile suggests that there is still some homodimer present, a result also consistent with the SAXS analysis (Figure 5, column 5). In conclusion, both the NMR and SAXS analyses support the conclusions that the L289K mutation and acetonitrile reduce dimer stability.

Effect of Nevirapine and KCl on Dimerization and Thumb Subdomain Orientation. Addition of the NNRTI nevirapine strongly favors the open conformation of the fingers/thumb subdomains (46, 47), while inconsistent results have been obtained for the effect of nevirapine on dimerization (4, 30, 31). As demonstrated previously (38), the addition of nevirapine to the RT heterodimer results in large shift perturbations for the two active site methionine residues, M184₆₆ and M230₆₆ in the p66 subunit, while not perturbing any of the methionine residues in the p51 subunit. This result is reproduced in Figure 7a for [*methyl-¹³C*]methionine₅₁ RT (38). In our study, we found that nevirapine produces analogous changes when added to the isolated p51 subunit, interacting with the p51E subunit of the homodimer, and possibly with the p51E monomer, if this is present in solution (Figure 7b). Nevirapine also produces qualitatively similar but weaker effects on the spectrum of [*methyl-¹³C*]methionine p51_{L289K} (Figure 3d). We note that much of the M230 resonance intensity remains unshifted after the addition of the nevirapine (Figure 7b), consistent with the main contribution to this resonance from M230 in the compact, p51-like subunit of the heterodimer. In addition, there is probably also some resonance intensity from M357_B at this position. These results demonstrate the close similarity in the active site structures and NNRTI interactions between the p66/p51 heterodimer and the p51 homodimer.

The effect of nevirapine, which can be evaluated by comparing columns 7 and 8 with columns 1 and 2 in Figure 5, is both to increase the total dimer fraction and to stabilize the open conformation of the fingers/thumb subdomains. At 60 μ M p51 and 500 μ M nevirapine, no monomer was present, and more than 60% of the dimer was in the open conformation, as expected from crystal structures with NNRTI's bound (46, 47). In addition, the nevirapine also counteracts much of the effect of the L289K mutation (compare columns 4 and 6), when the monomer concentration is reduced from 66 to 4%.

We also have evaluated the effects of ionic strength (KCl) on p51 dimerization. The SAXS data were described well using a mixture of only two component species: the p51C monomer and the p51E_{closed}/p51C dimer, with the dimer fraction showing a monotonic increase with KCl concentration (Figure 8). This dependence is similar to results obtained for p66 homodimer formation (26, 48) and also is consistent with the large hydrophobic interface between the two subunits (29, 45).

Equilibrium Modeling of the Effect of the L289K Mutation on Dimerization. The surprising effects of the L289K mutation on p51 homodimer formation can be understood on the

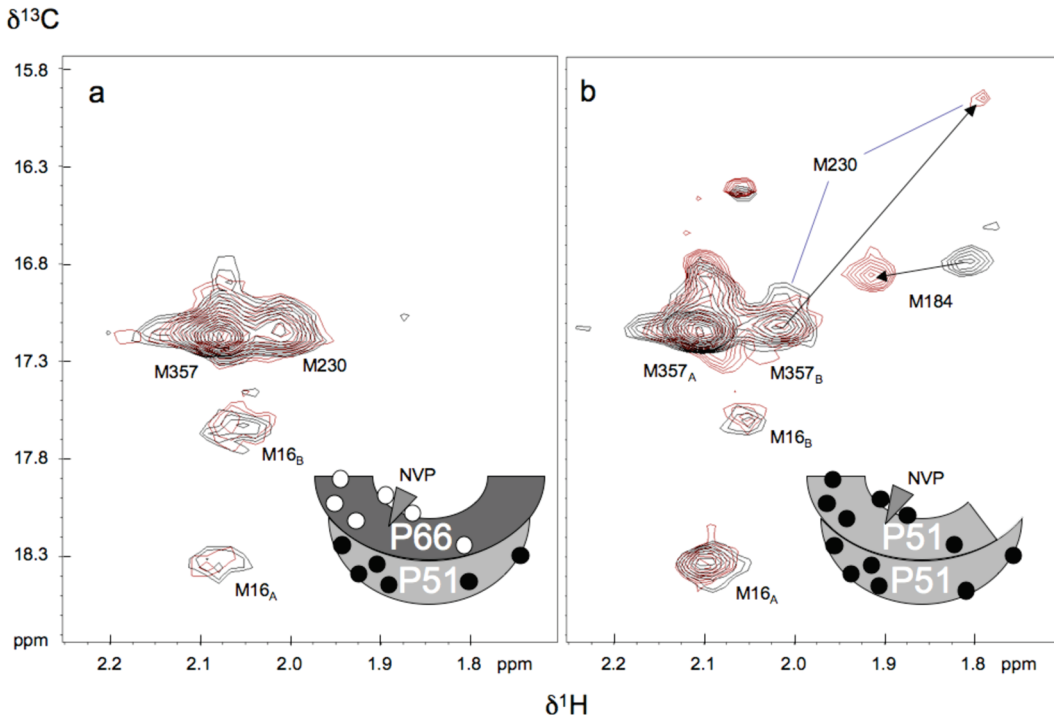


FIGURE 7: Effect of nevirapine on p51 NMR spectra. (a) ^1H - ^{13}C HSQC spectra of [$\text{methyl}^{13}\text{C}$]methionine₅₁ RT (50 μM) in the absence (black) and presence (red) of 200 μM nevirapine. (b) ^1H - ^{13}C HSQC spectra of uncomplexed [$\text{methyl}^{13}\text{C}$]methionine p51 (30 μM) in the absence (black) and presence (red) of 100 μM nevirapine. The arrows indicate resonance shifts in response to nevirapine. NMR parameters and buffer as described in the legend of Figure 2. Schematic figures (inset) indicate the subunit labeling pattern, with filled circles indicating [$\text{methyl}^{13}\text{C}$]methionine labeling; the triangle at the active site represents nevirapine. The spectrum of the p66/p51 heterodimer preparation shown in panel a is reproduced from Figure 7c of ref 38. Preparation of the selectively labeled heterodimer is described in that reference.

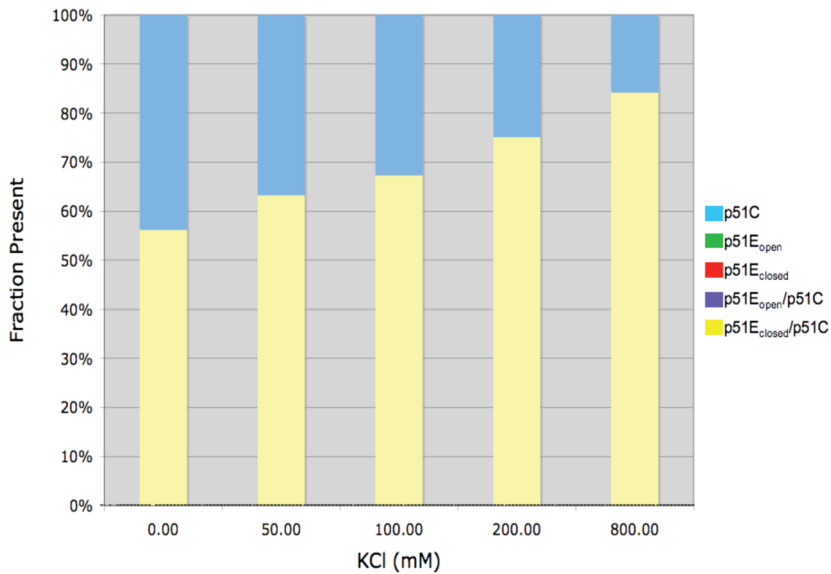


FIGURE 8: Effect of KCl on the p51C monomer:dimer ratio. Samples contained 50 μM p51_{C280S} in 50 mM Tris-HCl (pH 8.0), 4 mM MgCl₂, and the indicated concentrations of KCl. Fractional component concentrations were determined using OLIGOMER analysis of the SAXS data, as described in the legend of Figure 5. Only two species were observed under the conditions of the study: the cyan bars represent the compact monomer, p51C, and the yellow bars correspond to the dimer with a closed fingers/thumb conformation, p51E_{closed}/p51C.

basis of a conformational selection model outlined below. This model is based on the results summarized above showing that p51 samples contain predominantly p51C, a variable level of concentration- and condition-dependent homodimer, and no other significantly populated species. We assume that the p51 monomer can exist in either of two conformations, p51C and p51E, and the only stable dimer that can exist is the conformational heterodimer, p51E/p51C. The dimerization process is thus

described by these two equilibrium equations:



Figure 9a shows a representative calculation for the fractions of the three molecular species, p51C, p51E, and p51E/p51C, as a

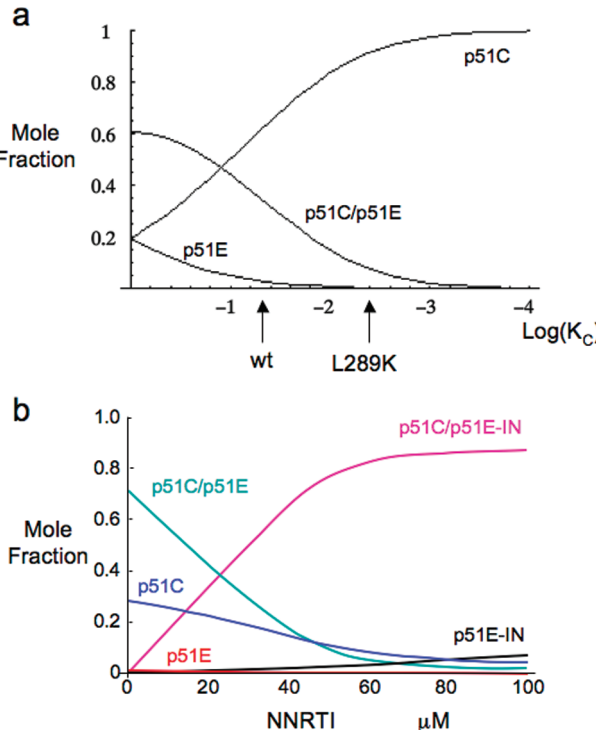


FIGURE 9: Illustrative numerical calculations of molecular species concentrations based on a conformational selection dimerization model. (a) The fractional p51C, p51E, and dimeric p51E/p51C concentrations are calculated as a function of K_C for the following parameters: K_D = 2 μ M, and p51_T = 50 μ M. The K_C values that would approximately correspond to wt and to L289K mutant p51 are indicated. (b) Molecular species determined as a function of NNRTI concentration for the model shown in Scheme 1. The calculation corresponds to the following parameters: p51_T = 100 μ M, K_C = 0.03, K_D = K_{D2} = 0.2 μ M, and K_I = K_{I2} = 1.0 μ M. Thus, for the calculation shown, the binding of the inhibitor does not contribute directly to the affinity of the monomers, but only indirectly, through the effect on the conformational distribution of p51 monomers.

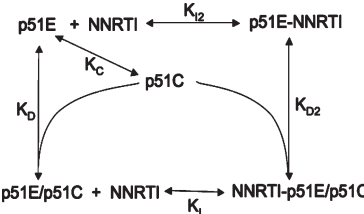
function of the equilibrium constant K_C. The calculation sets K_D equal to 2 μ M and the total concentration of p51 (p51_T) to 50 μ M to reproduce the large amount of dimer that is observed experimentally. This value is much lower than the recently reported p51 homodimerization K_D of 230 μ M (5) due to the different definition used and to the differences in experimental conditions. The studies of Venezia et al. (5) were performed at 5 °C in 50 mM Tris (pH 7.5), 10% (v/v) glycerol, and 25 mM NaCl, and it has been shown that the association rate constant for the heterodimer is strongly dependent on both temperature and Mg concentration (28, 29), both of which are substantially higher in our study. To summarize, the calculation described above introduces an explicit dependence of the dimerization process on the relative stabilities of the two p51 conformations that constitute the p51 homodimer.

According to the conformational selection model outlined above, a preexisting p51E conformation is stabilized by the interaction with p51C. The explicit temperature dependence of the equilibrium ratio of p51E/p51C is given by

$$K_C = \frac{p51E}{p51C} = e^{-\Delta G/kT} \quad (3)$$

The complete absence of any p51E species over a range of experimental conditions used in the SAXS studies summarized in Figure 5 indicates that ΔG is at least several kilocalories per

Scheme 1



mole, and very possibly much larger. A larger ΔG would in general be consistent with slower association kinetics, although in principle, such effects can also result from a large activation energy barrier required for the p51C to p51E transition. Higher ΔG values, leading to lower K_C values, require correspondingly lower K_D values to explain the observed dimer concentrations. Low K_D values are qualitatively consistent with the large buried surface area of 3000 Å² calculated for the p51 homodimer (45). For example, setting the total p51 concentration p51_T to 50 μ M, K_C to 0.1, and K_D to 1 μ M, one obtains 55% dimer, 41% p51C, and 4% p51E, while lowering K_C to 10⁻⁴ requires a K_D value of 1 nM to produce a similar dimer fraction. As noted above, no p51E was detected in any of the SAXS studies (Figures 5 and 8).

Within the context of the model described above, we suggest that the effect of the L289K mutation is to further stabilize the p51C conformation by replacing a solvent-exposed leucine residue with a lysine, thus further lowering the value of K_C ([p51E]/[p51C]) (Supporting Information). Consistent with this discussion, we propose that this mutation would have little direct effect on K_D, while it would significantly stabilize p51C, resulting in a lower K_C value. The estimated effect of the L289K mutation on the equilibrium distribution of p51C, p51E, and p51C/p51E is indicated by the arrow in Figure 9a.

Equilibrium Modeling of the Interaction of p51 with an NNRTI. We have generalized the equilibrium model described above to evaluate the effects of NNRTI binding, and in principle the effect of any agent whose affinity shows a strong conformational dependence. As in the model developed in the preceding section, p51 is allowed to adopt two conformations: p51E and p51C. The equilibrium constants K_C and K_D have the same definition as in the preceding discussion. Since, according to this model, p51 is capable of adopting a p66-like conformation, it is also capable of forming the NNRTI binding pocket and interacting with NNRTIs. In addition, p51C and p51E with or without NNRTI are allowed to dimerize (Scheme 1). The equilibrium condition requires that the corresponding equilibrium constants be related according to (Supporting Information)

$$\frac{K_{I2}}{K_I} = \frac{K_D}{K_{D2}} \quad (4)$$

An illustrative calculation of the dependence of the molecular species on the NNRTI concentration is shown in Figure 9b. In the absence of the inhibitor, three species are present: p51C, p51E, and p51E/p51C dimer. Addition of the NNRTI results in the formation of two additional species (p51E-NNRTI and NNRTI-p51C) and to compensatory decreases in the levels of p51C, p51E, and p51E/p51C (unliganded dimer). In the calculation shown in Figure 9b, we have set K_C equal to 0.03, so that p51C ≫ p51E, consistent with the results of the SAXS experiments (Figure 5). We also set K_I equal to K_{I2}, so that the affinity of the NNRTI for p51E is independent of whether the interaction is with the p51E monomer or the p51E/p51C dimer.

On the basis of the equilibrium constraint (eq 4), this also requires that the affinity of p51E for p51C to form the dimer be equal to the affinity of the p51E–NNRTI species for p51C. Thus, the entire effect on dimer formation shown in Figure 9b results from the effect of the NNRTI on the conformational distribution of the p51 monomer, and not from a preference for binding to the dimer.

According to the model of Scheme 1, the NNRTI can influence p51 homodimer formation in two ways. (1) It can stabilize (or, for some NNRTIs, destabilize) the dimer by altering the structure of the subunit interface, and thus K_D . (2) It can influence dimerization indirectly by altering the conformational distribution of the monomer through an effect on K_C . Formation of the p51E–NNRTI complex results in a second pathway favoring dimer formation. In this way, the NNRTI is predicted to exert an effect that opposes the effect of the L289K mutation, consistent with the SAXS data (Figure 5). The affinity of Mg for the active site aspartyl residues of p51E suggests that it should promote homodimer formation in a manner that is analogous to the effect of the NNRTI. This effect is consistent with the reported effects of Mg on dimerization (8), although we note that Mg can also influence this process as a result of a change in ionic strength, similar to the effect shown for KCl (Figure 8). Another way of considering this effect is that the subunit binding energy that would be required for maturation of the dimer complex does not have to be expended to the extent that a preformed p51E–NNRTI complex is available which more closely approximates the p51E conformation present in the mature complex.

DISCUSSION

Dimerization of HIV reverse transcriptase is an essential step required for obtaining mature, active enzyme. It can be influenced by mutations (15–25), non-nucleoside reverse transcriptase inhibitors (4–6), solution conditions (8, 27–29), and small molecule dimerization inhibitors developed specifically for this purpose (7, 9–14, 28, 49). The p51 subunit represents a useful model system for the behavior of the RT heterodimer since it exhibits a significant level of homodimer-dependent polymerase activity (32, 50) as well as analogous dimerization behavior. Further, the observation of significant polymerase activity has been used to infer that one of the subunits of the p51 homodimer must adopt a p66-like conformation (50). Alternatively, multiple studies have demonstrated that the primer/template substrate used for activity measurements can significantly lower the apparent K_D for formation of both homo- and heterodimer (8, 26, 29, 33). Thus, these activity-dependent measurements do not necessarily indicate that the p51 homodimer is present in the absence of primer/template substrates. Comparison of the KCl effects on the activity of the p51 homodimer (32) with the KCl-dependent dimerization observed in the SAXS studies indicates that an increased level of dimerization is not necessarily associated with increased activity, presumably as a consequence of the interference of high ionic strength with primer/template binding. On the basis of a radiation target analysis study, Sluis-Cremer et al. (33) determined that the p51 homodimer could be observed only in the presence of a DNA primer/template. This conclusion is, however, at odds with other studies based on size-exclusion chromatography (27) and sedimentation equilibrium (5), according to which the p51 dimer was observed in the absence of nucleotide substrates.

In the present study, the NMR spectra of [*methyl-¹³C*]-methionine p51 studied at a total monomer concentration of 30 μ M in 200 mM KCl and 4 mM MgCl₂ show several features that are unequivocally associated with a p66-like, p51E conformation (e.g., Figure 1c). The conclusion that a p66-like conformation is present, even in the absence of a primer/template motif, is further strengthened by the observation that the spectral perturbations induced by nevirapine in the sample containing only p51 are essentially identical with those observed in the methionine-labeled p66/p51 heterodimer (Figure 7). The NMR spectra therefore demonstrate the presence of a mixture that contains both the p51C and p51E species but provide limited evidence of the degree of dimer formation. The SAXS analysis resolves this issue, providing a satisfactory fit for a binary mixture of the p51C monomer and a p51E_{closed}/p51C dimer in which the fingers/thumb subdomains adopt a closed conformation. Importantly, there is no evidence of a significant concentration of the p51E monomer under any of the conditions studied. These observations do not completely rule out the presence of some p51E monomer or other oligomers as long as these correspond to only a small fraction of the molecular species present.

Although we cannot offer a precise explanation for the differences among these reported studies, it is clear that the high sensitivity of the dimerization process to the experimental conditions is the major reason for these apparent discrepancies. For example, Divita et al. have previously identified temperature (28, 29) and Mg (8) as critical factors for p66/p51 heterodimerization. These results are consistent with the substantially lower apparent K_D for p51 homodimer formation indicated by our observations at 25 °C compared with the recent K_D value determined at 5 °C with 10% glycerol based on equilibrium sedimentation (5). Cabodevilla et al. (26) found that p66 homodimer formation is strongly favored at higher ionic strengths, similar to our SAXS results for p51 homodimer formation (Figure 8). Although it is unclear why no evidence of a p51 homodimer was obtained in the previously reported radiation target analysis study (33), the lower temperature (20 °C), lower salt concentration (100 mM NaCl), and apparent absence of Mg (which was present for the activity measurements) would have contributed to a reduced fractional dimer concentration.

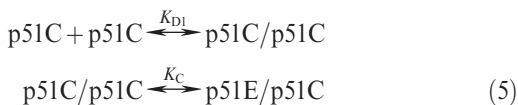
Conclusions regarding the effects of the NNRTI nevirapine on homodimer formation have also been inconsistent (4, 30, 31). The SAXS studies presented here demonstrate a significant nevirapine-induced enhancement of p51/p51 homodimer formation under the conditions used here (Figure 5). In addition to the effects on the wild-type enzyme, nevirapine is able to significantly counteract the effects of the L289K mutation on dimerization (Figure 5).

The validity of the SAXS analysis is supported primarily by the qualitative consistency of the effects of different experimental conditions with expectations based on the limited literature for p51 and the more extensive literature for p66 and the p66/p51 dimer. The observed high fractional concentration of p51C is consistent with the analysis of Wang et al. (45), who determined that formation of the compact p51C structure eliminates an extensive hydrophobic solvent interface, so that the monomeric forms of p51, as well as p66, are expected to have the structure observed for the p51 subunit of the heterodimer, i.e., p51C. The effect of nevirapine in selecting the open conformation of the fingers/thumb subdomains is also qualitatively consistent with multiple crystal structures of the nevirapine–p66/p51 complex (46, 47, 51–53). Alternatively, the preference of the

uncomplexed p51E/p51C dimer for a closed fingers/thumb orientation agrees with the results of ESR studies of spin-labeled RT (34) and indicates that the SAXS methodology provides a useful approach for this type of conformational analysis of RT. The qualitative effect of the L289K mutation in reducing the level of p66 homodimerization and p66/p51 heterodimerization (15) is similarly supported by the SAXS analysis. Thus, despite uncertainties about the details of the component structures used for the deconvolution, the qualitative consistency of the results with a large amount of experimental data provides strong support for the validity of the SAXS analysis.

The SAXS and NMR results demonstrating significant levels of both p51C and p51E/p51C in solution provide important insights into the possible mechanism of homodimer formation, supporting a conformational selection model in which the predominant p51C species is able to "select" the low concentration of p51E that is present to form a homodimer. The model provides an extremely attractive basis for understanding the effect of the L289K mutation on dimer formation; it is apparent that this substitution will alter the equilibrium constant K_C but unclear why it should influence K_D . We also have generalized the model to include the effects of NNRTI binding, which can be considered to result from a combination of direct effects exerted at the subunit interface and indirect effects resulting from perturbation of the p51E \leftrightarrow p51C conformational distribution. The acute effect of temperature on homodimer formation is more readily understood on the basis of a temperature-dependent monomer conformation, rather than an effect on the dimerization reaction. In general, we suggest that the hypersensitivity of the apparent dimerization equilibrium to temperature and Mg concentration results primarily from an effect on the K_C value.

The experimental data do not necessarily rule out several related alternative models in which an initial p51C/p51C homodimer might form, followed by selection or perhaps even induction of the p51E conformer:



For such a model to be valid, the p51C/p51C conformer would need to be sufficiently stable to persist long enough for one of the p51C subunits to undergo a major conformational rearrangement. At this point, we find no evidence of the presence of such p51C/p51C homodimers; however, the presence of a small percentage of such species would not be inconsistent with the SAXS analysis. Although most previous treatments of RT dimerization favor the initial formation of a weak complex followed by a slow induced fit to progress to the mature dimer (e.g., ref 28), Venezia et al. (54) have recently found that the association rate constant is slower than that previously indicated and concluded that a conformational selection model provides the most attractive explanation for the dimerization kinetics of RT.

Finally, our results support the analysis presented by Wang et al. (45) indicating that the p51 monomer should adopt a p51C conformation and are thus also consistent with the prediction that the p66 monomer should have a similar structure. On the basis of the stability of the isolated RNase H domain (55), the p66 monomer would thus exist primarily as two globular domains, p51C and RNase H, connected by a flexible linker, a result that appears to be consistent with limited proteolysis studies (56). Such a model also provides a basis for understanding the

inhibition of heterodimer formation by the L289K₆₆ mutation, analogous to the effect described here for p51 homodimerization.

ACKNOWLEDGMENT

We thank Dr. Lin Yang of the X9 beamline, at the National Synchrotron Light Source at Brookhaven National Laboratory, for assistance with data collection. Use of the X9 beamline is supported by the United States Department of Energy, Office of Science, Office of Basic Energy Sciences, under Contract DE-AC02-98CH10886.

SUPPORTING INFORMATION AVAILABLE

Fits of all the SAXS data presented in Figures 5 and 8, tabulated SAXS data results, apparent K_D values, $^1\text{H}-^{13}\text{C}$ HSQC spectra showing the effects of acetonitrile on p51, ribbon diagrams indicating the positions of the L289 residues in the p66/p51 heterodimer and the modeled p51/p51 homodimer, analytical solutions for eq 2 used to generate Figure 9a, and a proof of eq 4. This material is available free of charge via the Internet at <http://pubs.acs.org>.

REFERENCES

- Autran, B., Carcelain, G., Li, T. S., Blanc, C., Mathez, D., Tubiana, R., Katlama, C., Debre, P., and Leibowitch, J. (1997) Positive effects of combined antiretroviral therapy on CD4(+) T cell homeostasis and function in advanced HIV disease. *Science* 277, 112–116.
- Staszewski, S., Morales-Ramirez, J., Tashima, K. T., Rachlis, A., Skiest, D., Stanford, J., Stryker, R., Johnson, P., Labriola, D. F., Farina, D., Manion, D. J., and Ruiz, N. M. (1999) Efavirenz plus zidovudine and lamivudine, efavirenz plus indinavir, and indinavir plus zidovudine and lamivudine in the treatment of HIV-1 infection in adults. Study 006 Team. *N. Engl. J. Med.* 341, 1865–1873.
- Sluis-Cremer, N., Arion, D., Abram, M. E., and Parniak, M. A. (2004) Proteolytic processing of an HIV-1 pol polyprotein precursor: Insights into the mechanism of reverse transcriptase p66/p51 heterodimer formation. *Int. J. Biochem. Cell Biol.* 36, 1836–1847.
- Tachedjian, G., Orlova, M., Sarafianos, S. G., Arnold, E., and Goff, S. P. (2001) Nonnucleoside reverse transcriptase inhibitors are chemical enhancers of dimerization of the HIV type 1 reverse transcriptase. *Proc. Natl. Acad. Sci. U.S.A.* 98, 7188–7193.
- Venezia, C. F., Howard, K. J., Ignatov, M. E., Holladay, L. A., and Barkley, M. D. (2006) Effects of efavirenz binding on the subunit equilibria of HIV-1 reverse transcriptase. *Biochemistry* 45, 2779–2789.
- Srivastava, S., Sluis-Cremer, N., and Tachedjian, G. (2006) Dimerization of human immunodeficiency virus type 1 reverse transcriptase as an antiviral target. *Curr. Pharm. Des.* 12, 1879–1894.
- Morris, M. C., Robert-Hebmann, V., Chaloin, L., Mery, J., Heitz, F., Devaux, C., Goody, R. S., and Divita, G. (1999) A new potent HIV-1 reverse transcriptase inhibitor. A synthetic peptide derived from the interface subunit domains. *J. Biol. Chem.* 274, 24941–24946.
- Divita, G., Restle, T., and Goody, R. S. (1993) Characterization of the dimerization process of HIV-1 reverse transcriptase heterodimer using intrinsic protein fluorescence. *FEBS Lett.* 324, 153–158.
- Divita, G., Restle, T., Goody, R. S., Chermann, J. C., and Baillon, J. G. (1994) Inhibition of human immunodeficiency virus type 1 reverse transcriptase dimerization using synthetic peptides derived from the connection domain. *J. Biol. Chem.* 269, 13080–13083.
- Camarasa, M. J., Velazquez, S., San-Felix, A., Perez-Perez, M. J., Bonache, M. C., and De Castro, S. (2006) TSAO derivatives, inhibitors of HIV-1 reverse transcriptase dimerization: Recent progress. *Curr. Pharm. Des.* 12, 1895–1907.
- Sluis-Cremer, N., Hamamouch, N., San Felix, A., Velazquez, S., Balzarini, J., and Camarasa, M. J. (2006) Structure-activity relationships of [2',5'-bis-O-(tert-butylidimethylsilyl)-β-D-ribofuranosyl]-3'-spiro-5''-(4''-amino-1'',2''-oxathiole-2'',2''-dioxide)thymine derivatives as inhibitors of HIV-1 reverse transcriptase dimerization. *J. Med. Chem.* 49, 4834–4841.
- Depollier, J., Hourdou, M. L., Aldrian-Herrada, G., Rothwell, P., Restle, T., and Divita, G. (2005) Insight into the mechanism of a peptide inhibitor of HIV reverse transcriptase dimerization. *Biochemistry* 44, 1909–1918.

13. Grohmann, D., Corradi, V., Elbasyouny, M., Baude, A., Horenkamp, F., Laufer, S. D., Manetti, F., Botta, M., and Restle, T. (2008) Small molecule inhibitors targeting HIV-1 reverse transcriptase dimerization. *ChemBioChem* 9, 916–922.
14. Agopian, A., Gros, E., Aldrian-Herrada, G., Bosquet, N., Clayette, P., and Divita, G. (2009) A new generation of peptide-based inhibitors targeting HIV-1 reverse transcriptase conformational flexibility. *J. Biol. Chem.* 284, 254–264.
15. Goel, R., Beard, W. A., Kumar, A., Casas-Finet, J. R., Strub, M. P., Stahl, S. J., Lewis, M. S., Bebenek, K., Becerra, S. P., and Kunkel, T. A.; et al. (1993) Structure/function studies of HIV-1(1) reverse transcriptase: Dimerization-defective mutant L289K. *Biochemistry* 32, 13012–13018.
16. Ghosh, M., Jacques, P. S., Rodgers, D. W., Ottman, M., Darlix, J. L., and Le Grice, S. F. (1996) Alterations to the primer grip of p66 HIV-1 reverse transcriptase and their consequences for template-primer utilization. *Biochemistry* 35, 8553–8562.
17. Wohrl, B. M., Krebs, R., Thrall, S. H., Le Grice, S. F., Scheidig, A. J., and Goody, R. S. (1997) Kinetic analysis of four HIV-1 reverse transcriptase enzymes mutated in the primer grip region of p66. Implications for DNA synthesis and dimerization. *J. Biol. Chem.* 272, 17581–17587.
18. Tachedjian, G., Aronson, H. E., and Goff, S. P. (2000) Analysis of mutations and suppressors affecting interactions between the subunits of the HIV type 1 reverse transcriptase. *Proc. Natl. Acad. Sci. U.S.A.* 97, 6334–6339.
19. Sluis-Cremer, N., and Tachedjian, G. (2002) Modulation of the oligomeric structures of HIV-1 retroviral enzymes by synthetic peptides and small molecules. *Eur. J. Biochem.* 269, 5103–5111.
20. Auwerx, J., Van Nieuwenhove, J., Rodriguez-Barrios, F., de Castro, S., Velazquez, S., Ceccherini-Silberstein, F., De Clercq, E., Camarasa, M. J., Perno, C. F., Gago, F., and Balzarini, J. (2005) The N137 and P140 amino acids in the p51 and the P95 amino acid in the p66 subunit of human immunodeficiency virus type 1 (HIV-1) reverse transcriptase are instrumental to maintain catalytic activity and to design new classes of anti-HIV-1 drugs. *FEBS Lett.* 579, 2294–2300.
21. Balzarini, J., Auwerx, J., Rodriguez-Barrios, F., Chedad, A., Farkas, V., Ceccherini-Silberstein, F., Garcia-Aparicio, C., Velazquez, S., De Clercq, E., Perno, C. F., Camarasa, M. J., and Gago, F. (2005) The amino acid Asn136 in HIV-1 reverse transcriptase (RT) maintains efficient association of both RT subunits and enables the rational design of novel RT inhibitors. *Mol. Pharmacol.* 68, 49–60.
22. Mulky, A., Sarafianos, S. G., Jia, Y., Arnold, E., and Kappes, J. C. (2005) Identification of amino acid residues in the human immunodeficiency virus type-1 reverse transcriptase tryptophan-repeat motif that are required for subunit interaction using infectious virions. *J. Mol. Biol.* 349, 673–684.
23. Mulky, A., Vu, B. C., Conway, J. A., Hughes, S. H., and Kappes, J. C. (2007) Analysis of amino acids in the β 7– β 8 loop of human immunodeficiency virus type 1 reverse transcriptase for their role in virus replication. *J. Mol. Biol.* 365, 1368–1378.
24. Wapling, J., Moore, K. L., Sonza, S., Mak, J., and Tachedjian, G. (2005) Mutations that abrogate human immunodeficiency virus type 1 reverse transcriptase dimerization affect maturation of the reverse transcriptase heterodimer. *J. Virol.* 79, 10247–10257.
25. Figueiredo, A., Zelina, S., Sluis-Cremer, N., and Tachedjian, G. (2008) Impact of residues in the nonnucleoside reverse transcriptase inhibitor binding pocket on HIV-1 reverse transcriptase heterodimer stability. *Curr. HIV Res.* 6, 130–137.
26. Caboche, J. F., Odrizola, L., Santiago, E., and Martinez-Irujo, J. J. (2001) Factors affecting the dimerization of the p66 form of HIV-1 reverse transcriptase. *Eur. J. Biochem.* 268, 1163–1172.
27. Restle, T., Muller, B., and Goody, R. S. (1990) Dimerization of human immunodeficiency virus type 1 reverse transcriptase. A target for chemotherapeutic intervention. *J. Biol. Chem.* 265, 8986–8988.
28. Divita, G., Rittinger, K., Geourjon, C., Deleage, G., and Goody, R. S. (1995) Dimerization kinetics of HIV-1 and HIV-2 reverse transcriptase: A two step process. *J. Mol. Biol.* 245, 508–521.
29. Divita, G., Rittinger, K., Restle, T., Immendorfer, U., and Goody, R. S. (1995) Conformational stability of dimeric HIV-1 and HIV-2 reverse transcriptases. *Biochemistry* 34, 16337–16346.
30. Sluis-Cremer, N., Dmitrienko, G. I., Balzarini, J., Camarasa, M. J., and Parniak, M. A. (2000) Human immunodeficiency virus type 1 reverse transcriptase dimer destabilization by 1-[spiro[4"-amino-2",2"-dioxo-1",2"-oxathiole-5",3"-[2',5'-bis-O-(tert-butyldimethylsilyl)- β -D-ribofuranosyl]]]-3-ethylthymine. *Biochemistry* 39, 1427–1433.
31. Tachedjian, G., Moore, K. L., Goff, S. P., and Sluis-Cremer, N. (2005) Efavirenz enhances the proteolytic processing of an HIV-1 pol polyprotein precursor and reverse transcriptase homodimer formation. *FEBS Lett.* 579, 379–384.
32. Bavand, M. R., Wagner, R., and Richmond, T. J. (1993) HIV-1 reverse transcriptase: Polymerization properties of the p51 homodimer compared to the p66/p51 heterodimer. *Biochemistry* 32, 10543–10552.
33. Sluis-Cremer, N., Kempner, E., and Parniak, M. A. (2003) Structure-activity relationships in HIV-1 reverse transcriptase revealed by radiation target analysis. *Protein Sci.* 12, 2081–2086.
34. Kensch, O., Restle, T., Wohrl, B. M., Goody, R. S., and Steinhoff, H. J. (2000) Temperature-dependent equilibrium between the open and closed conformation of the p66 subunit of HIV-1 reverse transcriptase revealed by site-directed spin labelling. *J. Mol. Biol.* 301, 1029–1039.
35. Studier, F. W. (2005) Protein production by auto-induction in high density shaking cultures. *Protein Expression Purif.* 41, 207–234.
36. Muchmore, D. C., McIntosh, L. P., Russell, C. B., Anderson, D. E., and Dahlquist, F. W. (1989) Expression and nitrogen-15 labeling of proteins for proton and nitrogen-15 nuclear magnetic resonance. *Methods Enzymol.* 177, 44–73.
37. Hou, E. W., Prasad, R., Beard, W. A., and Wilson, S. H. (2004) High-level expression and purification of untagged and histidine-tagged HIV-1 reverse transcriptase. *Protein Expression Purif.* 34, 75–86.
38. Zheng, X., Mueller, G. A., Derose, E. F., and London, R. E. (2009) Solution characterization of [methyl- 13 C]methionine HIV-1 reverse transcriptase by NMR spectroscopy. *Antiviral Res.* 84, 205–214.
39. Delaglio, F., Grzesiek, S., Vuister, G. W., Zhu, G., Pfeifer, J., and Bax, A. (1995) NMRPipe: A multidimensional spectral processing system based on UNIX pipes. *J. Biomol. NMR* 6, 277–293.
40. Johnson, B. A., and Blevins, R. A. (1994) Nmr View: A Computer Program for the Visualization and Analysis of Nmr Data. *J. Biomol. NMR* 4, 603–614.
41. Konarev, P. V., Volkov, V. V., Sokolova, A. V., Koch, M. H. J., and Svergun, D. I. (2003) PRIMUS: A Windows PC-based system for small-angle scattering data analysis. *J. Appl. Crystallogr.* 36, 1277–1282.
42. Svergun, D., Barberato, C., and Koch, M. H. J. (1995) CRYSTOL: A program to evaluate X-ray solution scattering of biological macromolecules from atomic coordinates. *J. Appl. Crystallogr.* 28, 768–773.
43. Spallarossa, A., Cesaroni, S., Ranise, A., Ponassi, M., Unge, T., and Bolognesi, M. (2008) Crystal structures of HIV-1 reverse transcriptase complexes with thiocarbamate non-nucleoside inhibitors. *Biochem. Biophys. Res. Commun.* 365, 764–770.
44. Bauman, J. D., Das, K., Ho, W. C., Baweja, M., Himmel, D. M., Clark, A. D., Oren, D. A., Boyer, P. L., Hughes, S. H., Shatkin, A. J., and Arnold, E. (2008) Crystal engineering of HIV-1 reverse transcriptase for structure-based drug design. *Nucleic Acids Res.* 36, 5083–5092.
45. Wang, J., Smerdon, S. J., Jager, J., Kohlstaedt, L. A., Rice, P. A., Friedman, J. M., and Steitz, T. A. (1994) Structural basis of asymmetry in the human immunodeficiency virus type 1 reverse transcriptase heterodimer. *Proc. Natl. Acad. Sci. U.S.A.* 91, 7242–7246.
46. Smerdon, S. J., Jager, J., Wang, J., Kohlstaedt, L. A., Chirino, A. J., Friedman, J. M., Rice, P. A., and Steitz, T. A. (1994) Structure of the binding site for nonnucleoside inhibitors of the reverse transcriptase of human immunodeficiency virus type 1. *Proc. Natl. Acad. Sci. U.S.A.* 91, 3911–3915.
47. Ren, J., Esnouf, R., Garman, E., Somers, D., Ross, C., Kirby, I., Keeling, J., Darby, G., Jones, Y., and Stuart, D.; et al. (1995) High resolution structures of HIV-1 RT from four RT-inhibitor complexes. *Nat. Struct. Biol.* 2, 293–302.
48. Rowley, G. L., Ma, Q. F., Bathurst, I. C., Barr, P. J., and Kenyon, G. L. (1990) Stabilization and activation of recombinant human immunodeficiency virus-1 reverse transcriptase-P66. *Biochem. Biophys. Res. Commun.* 167, 673–679.
49. Andreola, M. L. (2009) Therapeutic potential of peptide motifs against HIV-1 reverse transcriptase and integrase. *Curr. Pharm. Des.* 15, 2508–2519.
50. Dufour, E., El Dirani-Diab, R., Boulme, F., Fournier, M., Nevinsky, G., Tarrago-Litvak, L., Litvak, S., and Andreola, M. L. (1998) p66/p51 and p51/p51 recombinant forms of reverse transcriptase from human immunodeficiency virus type 1: Interactions with primer tRNA(Lys3), initiation of cDNA synthesis, and effect of inhibitors. *Eur. J. Biochem.* 251, 487–495.
51. Kohlstaedt, L. A., Wang, J., Friedman, J. M., Rice, P. A., and Steitz, T. A. (1992) Crystal-Structure at 3.5 Angstrom Resolution of HIV-1 Reverse-Transcriptase Complexed with an Inhibitor. *Science* 256, 1783–1790.

52. Ren, J., Nichols, C., Bird, L., Chamberlain, P., Weaver, K., Short, S., Stuart, D. I., and Stammers, D. K. (2001) Structural mechanisms of drug resistance for mutations at codons 181 and 188 in HIV-1 reverse transcriptase and the improved resilience of second generation non-nucleoside inhibitors. *J. Mol. Biol.* **312**, 795–805.
53. Chamberlain, P. P., Ren, J., Nichols, C. E., Douglas, L., Lennerstrand, J., Larder, B. A., Stuart, D. I., and Stammers, D. K. (2002) Crystal structures of zidovudine- or lamivudine-resistant human immunodeficiency virus type 1 reverse transcriptases containing mutations at codons 41, 184, and 215. *J. Virol.* **76**, 10015–10019.
54. Venezia, C. F., Meany, B. J., Braz, V. A., and Barkley, M. D. (2009) Kinetics of association and dissociation of HIV-1 reverse transcriptase subunits. *Biochemistry* **48**, 9084–9093.
55. Pari, K., Mueller, G. A., DeRose, E. F., Kirby, T. W., and London, R. E. (2003) Solution structure of the RNase H domain of the HIV-1 reverse transcriptase in the presence of magnesium. *Biochemistry* **42**, 639–650.
56. Lowe, D. M., Aitken, A., Bradley, C., Darby, G. K., Larder, B. A., Powell, K. L., Purifoy, D. J., Tisdale, M., and Stammers, D. K. (1988) HIV-1 reverse transcriptase: Crystallization and analysis of domain structure by limited proteolysis. *Biochemistry* **27**, 8884–8889.